

Quantitative oscillator strengths for ionic fragmentation of C 1s and O 1s excited CO¹

A.C.O. Guerra, J.B. Maciel, C.C. Turci, R.C. Bilodeau, and A.P. Hitchcock

Abstract: Ionic photofragmentation of carbon monoxide following carbon 1s and oxygen 1s excitation has been measured quantitatively with tuned synchrotron light and time-of-flight mass spectrometry using a Wiley–McLaren apparatus modified with an additional ion lens for improved quantitative performance. The sensitivity of the apparatus to kinetic energy and angular distribution effects has been characterized for selected lens settings through ion trajectory simulations and experimental measurements. Three distinct modes of the added lens have been identified (focus, defocus, and maximum). The focus mode has the least sensitivity to details of the angular and ion kinetic energy distribution and, therefore, is the best mode for measuring quantitative partial ion and ion-pair yields. The defocus mode has the most sensitivity to angular and kinetic energy distributions and, therefore, is the mode that provides the most information about the kinematics of photofragmentation. Branching ratios for ion and ion-pair production in all positive ion fragmentation channels were recorded from 280 to 330 eV (C 1s) and from 520 to 570 eV (O 1s) in the “focus” mode. Quantitative oscillator strengths were derived by combining these branching ratios with absolute total ion yield spectra. The results are compared to literature values.

Key words: CO, time-of-flight mass spectrometry, inner-shell excitation, quantitative oscillator strengths, cross sections.

Résumé : On a mesuré quantitativement le photofragmentation ionique du monoxyde de carbone qui suit les excitations 1s du carbone et 1s de l’oxygène à l’aide d’un rayonnement synchrotron et un spectromètre de masse à temps d’envol utilisant un appareil Wiley–McLaren modifié par l’addition d’une lentille ionique afin d’en améliorer la performance quantitative. Utilisant des simulations de trajectoires ioniques et des mesures expérimentales, on a caractérisé la sensibilité de l’appareil à l’énergie cinétique et aux effets de distribution angulaire pour divers ajustements choisis des lentilles. On a identifié trois modes distincts de lentilles ajoutées (focalisation, défocalisation et maximum). Le mode de focalisation est le moins sensible aux détails de la distribution de l’énergie angulaire et cinétique des ions et est donc le meilleur mode pour la mesure quantitative des rendements ioniques partiels et de paires d’ions. Le mode de défocalisation est le plus sensible aux distributions de l’énergie angulaire et cinétique et est donc le mode qui fournit le plus d’information concernant la cinématique de la photofragmentation. Les rapports de bifurcation dans la production de l’ion et de la paire d’ions dans les voies de fragmentation de tous les ions positifs ont été enregistrés de 280 à 330 eV (C 1s) et de 520 à 570 eV (O 1s) dans le mode de « focalisation ». On a dérivé les forces quantitatives de l’oscillateur en combinant ces rapports de bifurcation au spectre de rendement ionique total absolu. On compare les résultats aux valeurs rapportées dans la littérature.

Mots clés : CO, spectrométrie de masse en temps de vol, excitation de la couche interne, forces quantitatives de l’oscillateur, sections droites.

[Traduit par la Rédaction]

Introduction

Inner-shell excitation and associated decay spectroscopies are site-specific probes of electronic and geometrical structure and photoionization dynamics. Auger decay of inner-shell excited and ionized states is an efficient source of

multiply charged ions. The fragmentation of these species, studied by photoelectron – photoion – photoion coincidence (PEPIPICO) and photoion–photoion coincidence (PIPICO) spectroscopy (also called charge separation mass spectrometry), gives insight into bonding and electronic structure. In triatomic and larger polyatomic molecules, the dependence

Received 5 December 2003. Published on the NRC Research Press Web site at <http://canjchem.nrc.ca> on 14 September 2004.

A.C.O. Guerra. BIMR, Department of Chemistry, McMaster University, Hamilton, ON L8S 4M1, Canada and Instituto de Química, Universidade Federal do Rio de Janeiro, Rio de Janeiro, RJ 21949-900, Brazil.

J.B. Maciel and C.C. Turci. Instituto de Química, Universidade Federal do Rio de Janeiro, Rio de Janeiro, RJ 21949-900, Brazil.

R.C. Bilodeau.² Department of Physics, Western Michigan University, Kalamazoo, MI 49008, USA.

A.P. Hitchcock.³ BIMR, Department of Chemistry, McMaster University, Hamilton, ON L8S 4M1, Canada.

¹This article is part of a Special Issue dedicated to the memory of Professor Gerhard Herzberg.

²Present address: Lawrence Berkeley National Laboratory (ALS Division), 1 Cyclotron Road, Berkeley, CA 94720, USA.

³Corresponding author (e-mail: aph@mcmaster.ca).

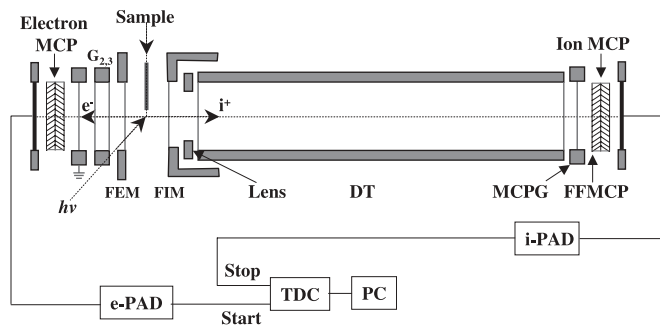
of the fragmentation process on the X-ray energy can reveal cases of site- and (or) state-selective fragmentation. The identification of potential candidates for selective X-ray photochemistry is an ongoing goal of our research program. To identify selectivity in fragmentation processes, quantitative yields are required, and thus it is important to understand the relationship between measured signals and the true partial photoionization cross sections (1). Some previous claims of selectivity in core level ionic fragmentation have been found to be, at least in part, an artefact of strong selectivity of the instrumentation to kinetic energy release distribution (KER or KERD) or angular distributions, combined with simultaneous changes of these factors among different core excited or ionized states (2).

To improve its quantitative performance, we have recently modified our Wiley–McLaren (3) time-of-flight (TOF) mass spectrometer to incorporate an ion-focussing lens (4). Here, we have used SIMION™ trajectory simulations (5) and experimental measurements of CO to investigate the sensitivity of the modified apparatus to kinetic energy and ion angle distributions. We have found the additional ion lens has produced an instrument with three distinct modes — maximum signal rate (maximum mode), minimum selectivity to angle and kinetic energy distributions (focus mode), and maximum selectivity to ion angle and kinetic energy distributions (defocus mode). The focus mode of our apparatus is shown to provide the most representative partial ion and ion-pair yields — i.e., those with the least distortions associated with varying kinetic energy or angular distributions, as judged by absence of structure in the ion and ion-pair yields for high kinetic energy ions. Photoelectron–photoion coincidence (PEPICO) and PIPICO measurements of the ionic fragmentation following C 1s and O 1s excitation and ionization of CO are used to demonstrate these modes. The CO molecule was chosen because its electronic spectroscopy and core level photofragmentation have been studied extensively, and because there have been several previous studies of the core level photofragmentation yields claiming quantitative results (6, 7). Photoionization mass spectroscopy (6–15), photoelectron spectroscopy (16, 17), electron–ion coincidence spectroscopy (18, 19), and electron energy loss spectroscopy (20–24) measurements on CO were performed. The results are compared to an early time-of-flight photoionization mass spectrometry study, in which a very short extraction pulse was used to improve quantitative collection (6), and to (e,e + ion) coincidence measurements (7) simulating photoionization, which are generally accepted to produce branching ratios free from kinetic energy distortion. We discuss our results relative to a wider range of partial ion yield results on CO (6, 7–11, 25).

Experimental

The experiments were performed using two different beamlines at the Synchrotron Radiation Center (SRC), University of Wisconsin at Madison. One was a modest resolution grasshopper monochromator (Mark II) equipped with a 1200 lines/mm grating. The other was the high-resolution spherical grating monochromator (SGM) of the Canadian Synchrotron Radiation Facility (CSRF). The X-ray beam

Fig. 1. Schematic diagram of the experimental TOF apparatus. Drift tube (DT), first electron mesh (FEM), first ion mesh (FIM), multichannel plate grid (MCPG, prevents ion feedback), microchannel plate (MCP), front electrode of the MCP (FFMCP), electron pre-amplifier, amplifier, discriminator (e-PAD), ion pre-amplifier, amplifier, discriminator (i-PAD), time-to-digital converter (TDC), personal computer (PC).

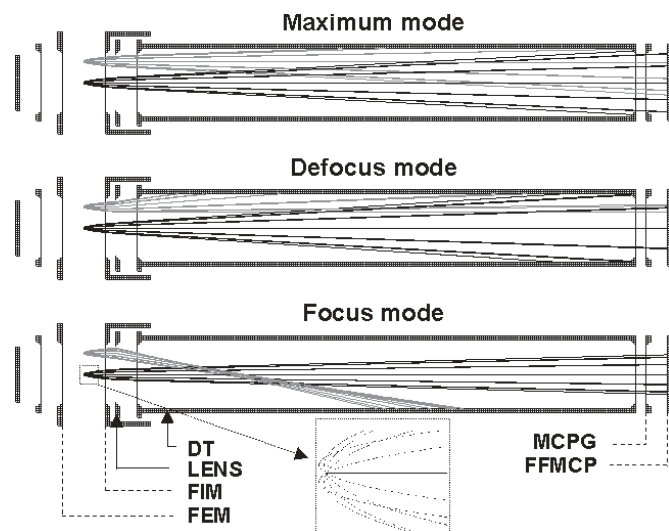


cross section in the ionization region was 2×1 mm in each case. For C 1s measurements, a 100 nm thin film of Ti was placed in the beam path to reduce second-order radiation by 70%. The sample was introduced into the experimental chamber as an effusive jet through a high-aspect-ratio stainless steel needle oriented perpendicular to both the time-of-flight (TOF) axis and the monochromatized photon beam. There was very little variation in gas density over the volume of the X-ray beam in the interaction region, as evidenced by negligible variation in signal strengths or spectral shapes as the position of the tip of the needle was varied over large ranges. Thus, signal is generated all along the X-ray beam path as it traverses the interaction region defined by the 25 mm mesh-covered openings into the electron detector and ion TOF drift tube. The sample pressure was maintained at $\sim 6 \times 10^{-6}$ torr (1 torr = 133.322 Pa) during data acquisition. The base pressure was $\sim 2 \times 10^{-8}$ torr so that residual gas signals contributed negligibly.

The TOF apparatus, prior to modification for addition of the ion lens, along with the PEPICO, PIPICO, and PEPICO modes, has been described earlier (1). Figure 1 shows a schematic diagram of the modified TOF apparatus, along with the electronic setup. It consists of a Wiley–McLaren type space charge focusing instrument (3) in which an electric field of up to 1050 V/cm (2000 V over 19 mm) was used to extract the parent and fragment ions. An additional lens (4) was installed between the drift tube (DT) and the ion extraction grid (FIM). The lens was designed to focus the fragment ions on a microchannel plate (MCP) detector.

Electrons and ions produced from photoionization were detected by two microchannel plate detectors (MCP), positioned directly opposite in relation to the TOF axis. Signals from the two MCP detectors were amplified and fed into LeCroy 688AL amplifier/discriminators. Coincidence detection was performed using an Ortec picosecond time analyzer (pTA) operated in a list mode, in which the arrival times of start (electron) and one or more stop (ion) signals were stored in a local memory and periodically downloaded to a microcomputer for further processing to generate the PEPICO, PIPICO, and other visualizations.

Fig. 2. C^+ ion trajectories computed by SIMIONTM, showing the existence of three modes of lens operation. Ions (20 eV) were started from the centre of the ionization region with initial ejection angles covering the full 360° (see insert figure at the bottom). One set of trajectories was started on the TOF axis and a second was started close to the edge of the entrance aperture into the drift tube. Potentials for the simulation: DT (−3800 V), FEM (+1000 V), FIM (−1000 V), MCPG (−3900 V), FFMCP (−3800 V), lens (−800 V for focus mode, −2200 V for maximum ion signal mode, and −3000 V for defocus mode).



Results and discussion

Characterization of the lens

Figure 2 shows the SIMIONTM simulations using potentials identified empirically for the instrument. The simulations are for the three different lens modes and an extraction field of 1050 V/cm (2000 V over 19 mm). The geometric parameters used in the simulation are listed in Table 1. For this geometry, the simulation flight times agree quite well with the measured times, indicating that the SIMIONTM model closely approximates the actual apparatus. The existence of the three modes was deduced from the SIMIONTM simulations, although the optimum lens voltages (summarized in Table 2) were found experimentally by determining optimal performance of each type — maximum ion signal for maximum mode; minimum kinetic energy discrimination, as evidenced by absence of the dip in the PIPICO signals, for “focus” mode; and maximum kinetic energy discrimination, as evidenced by the deepest dip in the PIPICO signals, for “defocus” mode. The PEPICO and PIPICO signals at 305 eV, for a 1050 V/cm extraction field and these three lens conditions, are compared in Fig. 3. The trajectories displayed in Fig. 2 are those of a positive ion with 20 eV kinetic energy, emitted at two points along the photon trajectory, one at the centre of the ionization region, the other 10 mm from the centre of the DT. The DT inner diameter is 25 mm, and thus the 10 mm off-centre starting point is still 2.5 mm away from the edge of the opening in the DT. Since the SIMIONTM geometry is a close approximation to the actual geometry, any edge effects not included in the simulation are expected to be minimal. From each of

Table 1. Geometric parameters used in the SIMIONTM simulations.

Geometric feature	Dimension in simulation (mm)
FEM–FIM gap	19.0
FIM lens and DT thickness	1.0
FIM (grid) – lens (front surface)	5.0
Lens (front surface) to DT (grid)	10.0
DT grid-to-grid	232.0

these points, a set of ion trajectories are plotted using take-off angles covering the full 360° (see insert to Fig. 2).

In the *focus* mode ($V_{\text{lens}} = -800$ V for $V_{\text{DT}} = -3800$ V), a convergent potential is used in which the ions emitted at any angle from a single spot are transported to the detector without loss, for all kinetic energies up to 20 eV. Of the three modes, this one provides the least kinetic energy or angular discrimination, and thus it should be the best for measuring representative partial ion yields, which can form the basis for quantitative partial ion yields. In the *defocus* mode ($V_{\text{lens}} = -3000$ V for $V_{\text{DT}} = -3800$ V), a divergent potential is used in which the ions emitted along the TOF axis from a wide range of lateral positions along the X-ray beam are transported to the detector. Ions starting with large off-axis angles tend to hit the walls. This mode provides the most information about on-axis kinetic energy distributions since the system has a narrow acceptance angle (approximately $\pm 30^\circ$). In the *maximum* mode, ions emitted all along the photon path are focused to the detector. The simulation shows that, for many positions along the photon path, an approximately $\pm 60^\circ$ acceptance angle is achieved at an extraction field of 1050 V/cm. Note that although, relative to the defocus mode, poorer kinetic energy distribution information results from the larger acceptance angle, the angle is better defined (all positions on the X-ray beam axis have the same angular distribution sampled), resulting in significantly larger signals (about 3 to 4 times more than in the focus or defocus modes).

PEPICO and PIPICO signals from CO in the three lens modes

Figure 3 shows the PEPICO and PIPICO signals for CO ionized at 305 eV, the peak of the excitation to the quasi-bound ($C\ 1s^{-1}, \sigma^*$) state, also called the σ^* shape resonance. The extraction field was 1050 V/cm and the lens voltages for the three modes are those for which the SIMIONTM calculations were performed. The first stop signal (from single and the faster ion produced in dissociative double ionization) and the second stop signal (from the slower ion of dissociative double ionization) have been summed in each case. The peak shapes of high kinetic energy species (C^{++}, O^{++}, C^+, O^+), and especially the PIPICO signals that correspond mostly to highly energetic ions, show significant changes between the focus and defocus modes. For example, $I(C^+)/I(O^+) > 1$ for the focus mode but $I(C^+)/I(O^+) < 1$ for the defocus mode ($I(x)$ = intensity of ion x). These changes are consistent with loss of fast C^+ ions, and thus much higher KER sensitivity in the defocus mode but very little KER or angular selectivity in the focus mode. The maximum mode gives a significantly higher signal in both PEPICO and

Table 2. Voltages and lens ratios for the three modes at the various extraction fields explored.

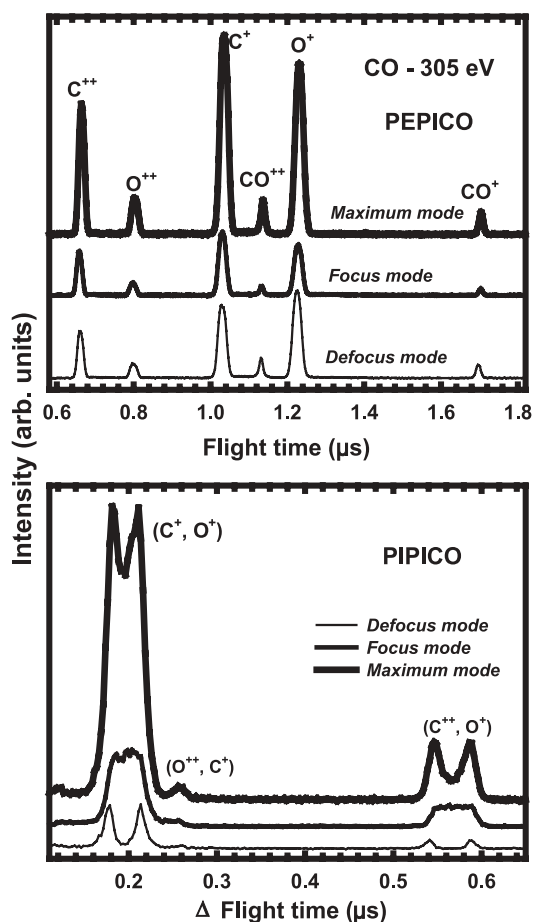
FEM (+V)	FIM (-V)	DT (-V)	Lens voltages (-V)			Lens ratios	
			Focus	Maximum	Defocus	V_d^a/V_f^b	V_d/V_m^c
120	120	600	80	200	300	3.75	1.50
200	200	950	150	400	550	3.67	1.38
300	300	1400	300	700	1000	3.33	1.43
500	500	2700	500	1150	1650	3.30	1.43
1000	1000	3800	800	2200	3000	3.75	1.36

^a V_d is the applied lens voltage used for defocus mode.

^b V_f is the applied lens voltage used for focus mode.

^c V_m is the applied lens voltage used for maximum mode.

Fig. 3. PEPICO (upper) and PIPICO (lower) spectra for C 1s ionized CO at 305 eV, measured with the lens set for focus, defocus, and maximum modes, as indicated in the legend. For clarity, the ordinates of the curves have been shifted with respect to each other. The intensities are in correct proportions.



PIPICO and has a KER discrimination somewhere in between the focus and defocus modes. Since the kinetic energy release distribution (KERD) is spread over more time at weak extraction fields and is thus easier to sample, it is often favorable to use the low extraction field to explore kinetic energy distributions and polarization-dependent ion yields. We stress the extremely flat-topped character of the (C^+, O^+) PIPICO signals in the focus mode. This is an unambiguous indication of the absence of angular discrimination and strongly supports our claim that this mode provides relative ion yields that are proportional to the quantitative ion yields.

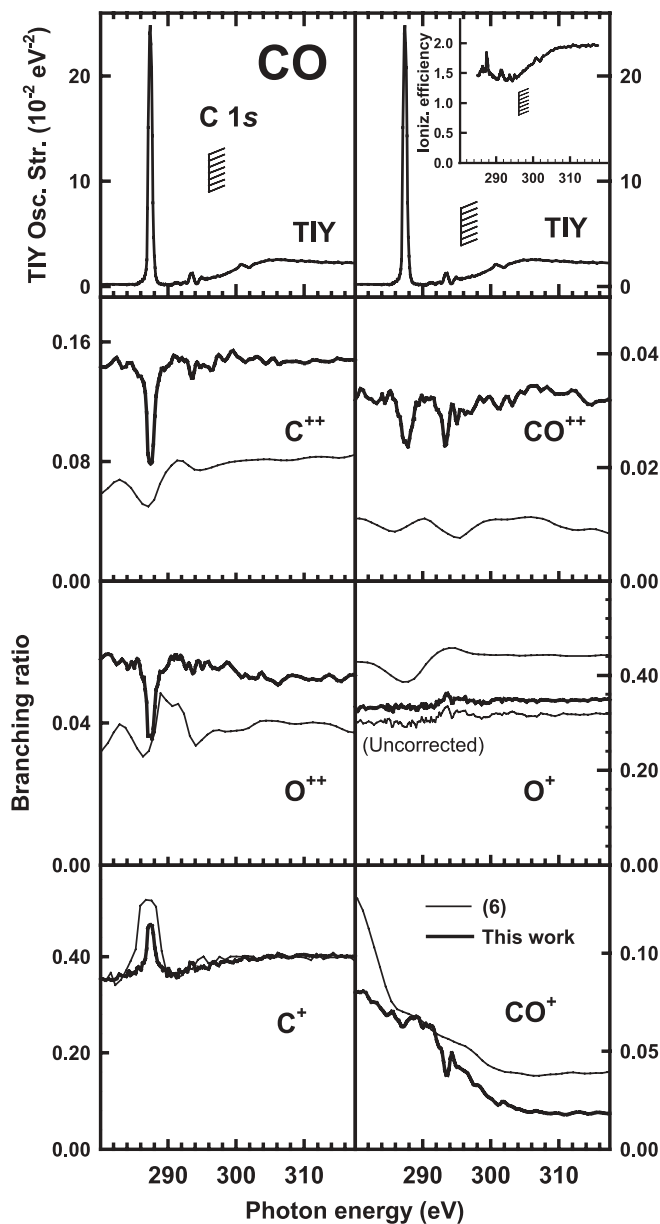
Experimental conditions with these three limiting behaviors could be found for a wide range of different extraction fields, indicating they are a fundamental aspect of the ion optics. Table 2 lists the voltages and lens ratios for the three modes at the various extraction fields explored. We chose to use an extraction field of 1050 V/cm to maximize the yield. Even below 200 V/cm extraction field, it is possible to see the characteristic changes in the TOF or PIPICO shapes seen in Fig. 3 as a function of lens voltages, indicating there are distinct modes, even under weak extraction field conditions. Within experimental error, the lens ratios V_d/V_f and V_d/V_m are independent of extraction fields (V_d , V_f , and V_m are the optimal lens voltages in defocus, focus, and maximum modes, respectively). This observation suggests to us that our experimental procedure used to define the optimal lens voltages is valid and that the conditions we are identifying in this manner are general properties of the lens, and not specific to a narrow range of extraction fields.

At 305 eV photon energy, the CO^+ yield is very small since this species only arises from the weak underlying valence shell ionization or from the even weaker fluorescence decay of the C 1s core hole. In fact, there is also a small contribution from CO^+ produced by low-energy UV stray light. Since virtually all of the 1s ion states decay by Auger, a final charge state of at least 2+ must exist. Although there is a small yield of CO^{++} , most of the CO^{++} states undergo symmetric dissociative double ionization producing C^+ and O^+ , as explained by the ‘‘Coulomb explosion’’ model (26). The C^+ and O^+ signals from core ionization are very similar and dominate the spectra. These signals arise mainly from (C^+, O^+) ion-pair production (6). The yields of C^{++} and O^{++} are likely associated with asymmetric dissociation, although some also arise from the weak triple ionization processes producing (C^{++}, O^+) or (O^{++}, C^+) ion pairs detected in the PIPICO and PEPICO measurements.

Photoion branching ratios

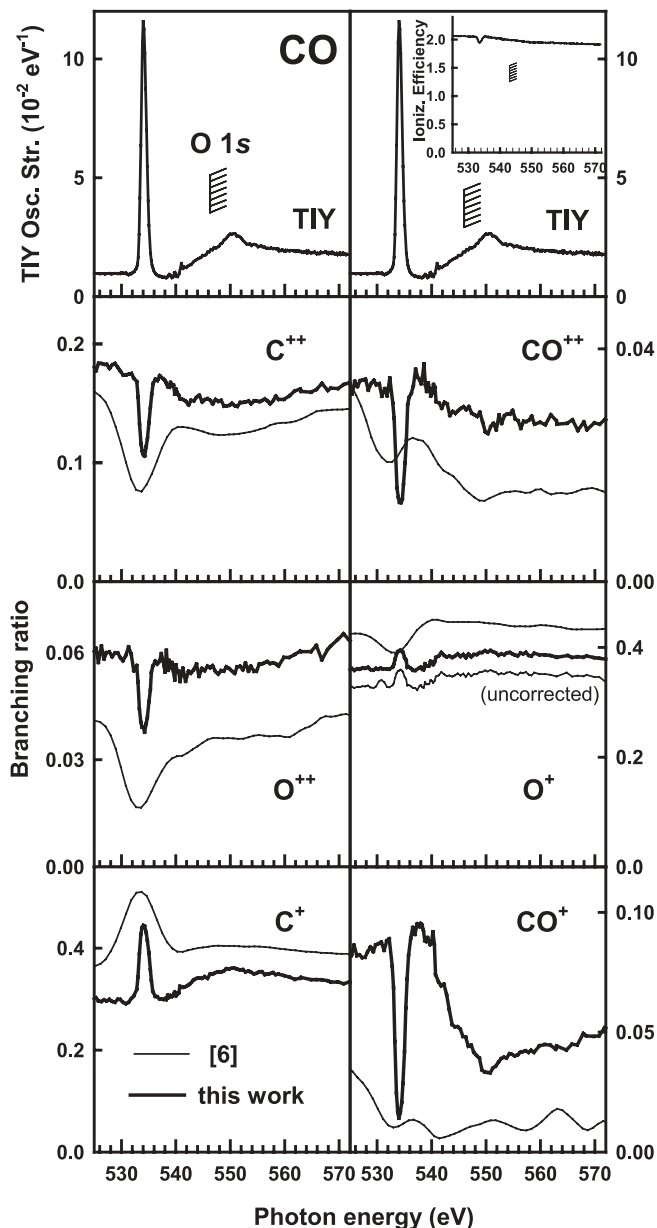
The branching ratio (BR) is the ratio of the yield of a specific ion to the total ion yield. Figure 4 shows the C 1s photoion branching ratios between 280 and 320 eV measured in the focus mode, as compared to literature values (6). The branching ratio data shown in Fig. 4 are the average from two sets of measurements. The curves for each ion were derived from the peak areas in the PEPICO spectra measured at a series of energies, with high extraction fields and the focus mode of the lens. After subtraction of the background of accidental coincidences, the first stop and second stop signals were summed to generate the branching

Fig. 4. Branching ratios for positive ion production from CO in the C 1s region derived from PEPICO mass spectra recorded with a Mark II grasshopper monochromator, as compared to literature values (6), which were digitized. The top of each column displays the total ion yield (TIY) spectra measured simultaneously and placed on an absolute scale, taking into account the estimated ionization efficiency of 2 in the C 1s continuum. The inset figure in the upper right panel is the estimated ionization efficiency. The O⁺ curve marked uncorrected is prior to addition of 20% of the C⁺ signal (followed by renormalization of all branching ratios to sum to unity). This correction compensates the fraction of the O⁺ signal lost because of masking by first arrival of a C⁺ signal. (A similar correction was applied in ref. 6.)



ratio. However, because the efficiency of ion detection is low (estimated to be 20%), this procedure does not account for the large loss of the O⁺ signal from the “masking” of that species by the C⁺ species for the (C⁺, O⁺) ion-pair process, which dominates the decay of C 1s ionized states. To compensate for the loss of the O⁺ signal, 20% of the signal from

Fig. 5. Branching ratios for positive ion production from CO in the O 1s region derived from PEPICO mass spectra recorded with the spherical grating monochromator, as compared to literature values (6). The top of each column displays the total ion yield (TIY) spectrum, with the oscillator strength scale set from published oscillator strength data (24, 27), taking into account the estimated ionization efficiency of 2 in this energy region. The O⁺ curve marked uncorrected is prior to the addition of 20% of the C⁺ signal (see caption to Fig. 4 for further details).



the C⁺ yield was added to the O⁺ yield and the branching ratios recomputed. Figure 4 plots both the uncorrected and corrected O⁺ branching yield spectra. Figure 5 shows the measured O 1s photoion branching ratios, derived from a sequence of PEPICO spectra measured in the 525–570 eV range with high extraction fields and the focus mode of the lens. As with the C 1s region, the O⁺ signal was augmented by 20% of the C⁺ signal to compensate for loss of the O⁺ from the dominant (C⁺, O⁺) ion-pair process.

Table 3. Branching ratios following soft X-ray photoionization of CO.

Ion	(Valence) ⁻¹			C 1s → 2π ^{*a}		
	280 eV (This work)	280 eV (Reference 6)	280 eV (Reference 7)	287.4 eV (This work)	287.4 eV (Reference 6)	287.4 eV (Reference 7)
C ⁺⁺	0.143(8) ^b	0.05	0.02	0.080(7)	0.03	0.05
O ⁺⁺	0.057(2)	0.03	0.01	0.042(2)	0.01	0.02
C ⁺	0.35(2)	0.35	0.22	0.46(2)	0.52	0.51
CO ⁺⁺	0.033(5)	0.01	0.02	0.025(5)	0.01	0.02
O ⁺	0.33(2)	0.46	0.26	0.33(2)	0.39	0.24
CO ⁺	0.080(7)	0.11	0.46	0.063(7)	0.05	0.17
O ⁺ +C ⁺	0.68(3)	0.81	0.48	0.79(3)	0.91	0.75
C ⁺ /O ⁺	1.06	0.76	0.85	1.39	1.33	2.1

^aBranching ratio at peak energy.

^bThe cited uncertainties are based on local statistical fluctuations in the data and do not reflect uncertainties associated with systematic errors.

The general shapes of the branching ratios are similar to those reported earlier, but there are differences in the quantitative yields. In particular, relative to ref. 6, in this work the yield of all doubly charged ion species is larger by 50%–100%, while that of the C⁺ and O⁺ singly charged species is about 20% smaller. This suggests that the earlier measurements underestimated the lower kinetic energy ion species. Note that the structure in the π^{*} region is much broader in the literature branching ratios (6) simply because of the poorer energy resolution of the earlier measurements (2.5 eV (6) vs. 0.6 eV fwhm (full width at half-maximum) in C 1s; 5 eV (6) vs. 1.5 eV fwhm in O 1s).

Figures 4 and 5 each include the total ion yield spectrum at the top of each column to help in the location of the states. This signal was measured simultaneously with the photoionization yields. For the O 1s spectrum, a small signal from impurity O₂ was subtracted (the O₂ π^{*} signal at 530.8 eV was about 3% of the CO π^{*} signal). Both C 1s and O 1s signals are set on an absolute oscillator strength scale by matching to earlier absorption oscillator strengths (6, 7, 24, 27), with a correction for the ionization efficiency, which is taken to be two above the C 1s ionization potential (6).

The inner-shell spectroscopy of CO has been described previously (6, 24) and is not controversial. Briefly, for the C 1s spectrum, the first strong peak at 287.4 eV is due to the C 1s → 2π^{*} transition. The weak structures at 292.4 and 293.4 eV correspond to C 1s → 3s and C 1s → 3p Rydberg excitations, respectively. The 294.8 eV feature is assigned as the overlap of 4s and 3d Rydberg transitions. The C 1s ionization potential (IP) is 296.1 eV (10). The feature in the near continuum at 300.7 eV is assigned to double excitation, while the broad structure at 305 eV is the σ^{*} shape resonance. The O 1s spectral features are assigned similarly: 534.1 eV (O 1s → 2π^{*}), 539.1 eV (O 1s → 3s), 540.4 eV (O 1s → 3p), 541.7 eV (O 1s → 4s, 3d), 542.4 eV (IP) (10), and 550.6 eV (shape resonance).

The C 1s branching ratio spectra can generally be divided into five regions: that below the onset of C 1s excitation (<287 eV), the C 1s discrete region (287–296 eV), the region just above the C 1s ionization threshold (296–300 eV), the near continuum (300–320 eV), and the continuum above the shake-off threshold (>320 eV). In contrast to the essentially constant ion branching ratios in the core ionization continua, at the π^{*} resonance there are large increases in the

C⁺ yield and significant decreases in the C⁺⁺ and O⁺⁺ yields. Similar observations can be made about the O 1s branching ratios, although the pre-O1s-edge signal is characteristic of C 1s ionization, rather than valence ionization, as in the pre-C 1s-edge signal, and thus the change from below to above the O 1s IP is smaller.

The C 1s branching ratios are also compared to results from a dipole regime electron–ion (e,e + ion) experiment (7) (Table 3). We found considerable disagreement, which was unexpected, since such measurements are generally considered quantitative. The CO (e,e + ion) study was one of the very first performed with that apparatus. It would be interesting to see the results of a modern (e,e + ion) measurement of CO.

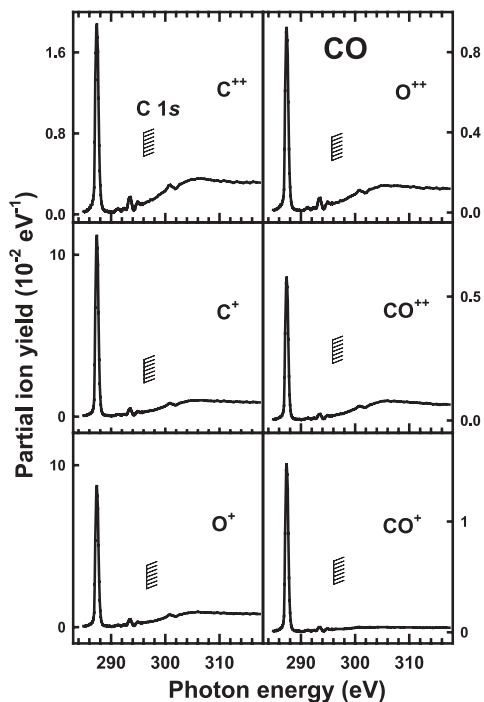
Table 3 presents branching ratios at selected energies derived from the quantitative focus mode, in comparison to literature values (6, 7). The I(C⁺)/I(O⁺) ratio for the C 1s π^{*} state is 1.39, very similar to the 1.33 value from ref. 6, but 34% lower than that from ref. 7. The I(C⁺)/I(O⁺) ratio for the O 1s π^{*} state is 1.12, as compared to 1.30 from ref. 6. As noted in ref. 6, these similar ratios in the C 1s and O 1s regions indicate that the site of the core hole in CO has relatively little influence on the final ion distribution for this molecule. The largest factor determining variation in the fragmentation pattern is discrete vs. continuum excitation, associated with essentially complete double ionization above the C 1s IP, but only partial double ionization below the IP.

Partial ion and ion-pair yields for CO

C 1s partial ion yields

Figure 6 presents the quantitative partial ion yield (PIY) spectra of C 1s excited – ionized CO from 280 to 320 eV, derived by taking the product of the branching ratio and the absolute total ion yield signal. The partial ion yield spectra of C⁺⁺, O⁺⁺, and CO⁺⁺ have enhanced continuum signals relative to the total ion yield (TIY). As found earlier (6), the C⁺⁺ and O⁺⁺ signals show a further rise at ~320 eV (not shown) corresponding to the onset of shake-off (simultaneous core and valence ionization) (6). The CO⁺ signal has negligible signal in the C 1s continuum since the only channel that can give rise to CO⁺ is fluorescence decay of the core hole, which has an extremely low probability. Note there is a very weak residual CO⁺ signal, amounting to less than 2% of the total signal, which is most likely from low-

Fig. 6. Quantitative partial ion yield (PIY) oscillator strength spectra of all positive ions produced from CO in the 280–320 eV region recorded in the focus mode.



energy UV stray light. The relative strength of the $C\ 1s \rightarrow 2\pi^*$ peak varies for the different ion products, indicating changes in the branching ratio for ionic fragmentation as discussed in the previous section and listed in Table 3.

O 1s partial ion yields

Figure 7 presents the quantitative PIY spectra of O 1s excited – ionized CO from 525 to 570 eV, derived by taking the product of the branching ratio and the absolute TIY signal. As with the C 1s partial ion yields, the yields of the doubly charged products are increased in the O 1s continuum, although the effect is less dramatic since the underlying signal arises mostly from C 1s ionization, where already the double ionization dominates. The CO^+ parent ion signal shows a constant contribution from underlying valence ionization, with additional yield at the $O\ 1s \rightarrow \pi^*$ transition and relatively more at the $O\ 1s \rightarrow$ Rydberg transitions, but no signal in the O 1s continuum.

C 1s and O 1s ion-pair yields

Figure 8 plots the branching ratios and the PIY spectra for the (C^+, O^+) and (C^{++}, O^+) ion pairs in the C 1s and O 1s regions derived from PIPICO data. The (C^+, O^+) ion-pair signal dominates the C 1s and O 1s continua. From the sum of the C^+ and O^+ branching ratios, we estimate that the ion-pair signal is 80% of the total ion signal. Since the TIY counts each ion separately, the derived total ion-pair yield (80% of the continuum TIY) was further divided by two to derive the oscillator strength for only ion-pair production. Thus, the absolute oscillator strength for producing the individual ion pairs was obtained by multiplying the ion-pair branching ratio times the TIY signal scaled by 0.40. (C^+, O^+) pair production is the strongest pair process in both core ionization

Fig. 7. Quantitative partial ion yield (PIY) oscillator strength spectra of all positive ions produced from CO in the 525–570 eV region recorded in the focus mode.

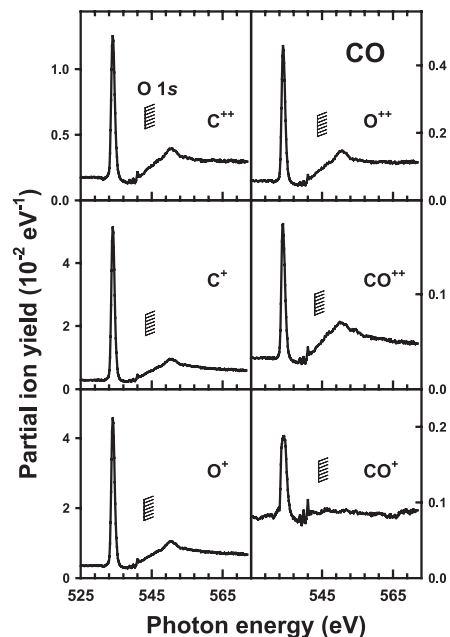


Fig. 8. Branching ratios (upper) and oscillator strength spectra (lower) for production of (C^+, O^+) and (C^{++}, O^+) ion pairs from CO in the C 1s and O 1s regions, derived from PIPICO spectra recorded with a high extraction field (1050 V/cm) and in the focus mode.

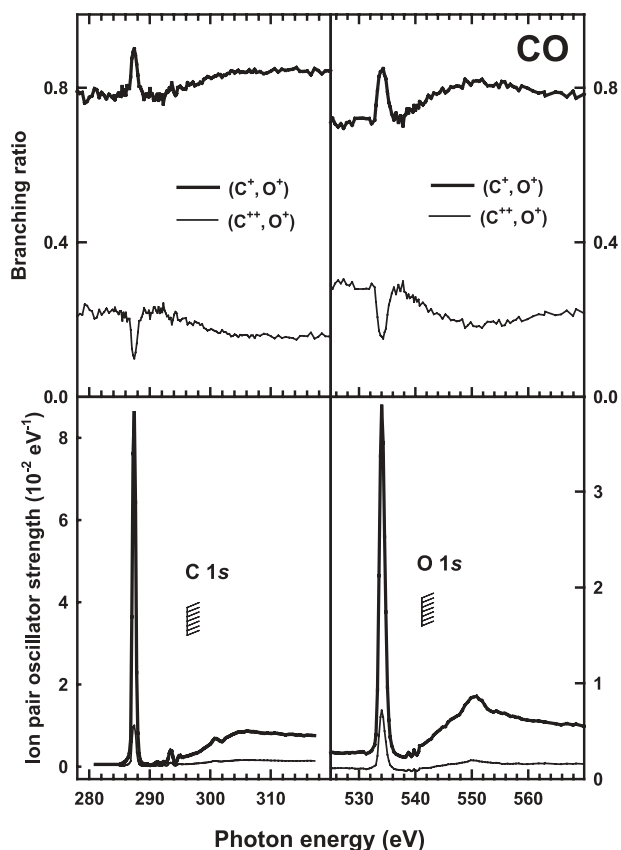
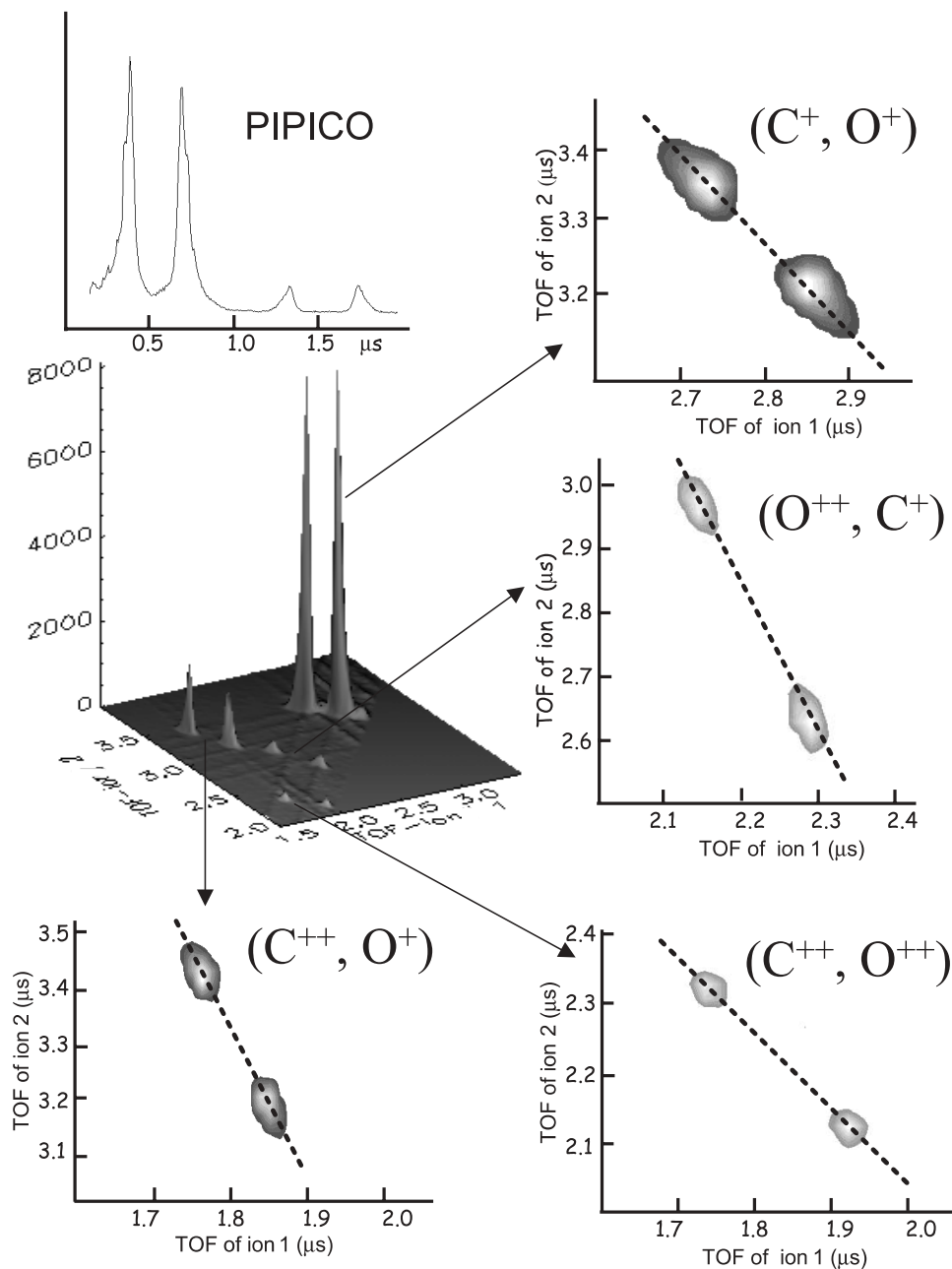


Fig. 9. PEPIPICO signals recorded in defocus mode at 305 eV with a weak extraction field (125 V/cm). The upper left curve is the PIPICO signal from the same data set.



continua. The dissociative triple ionization channel that produces the (C^{++}, O^+) pair constitutes $\sim 10\%$ of the total ion-pair signal, while the (O^{++}, C^+) signal, which is almost invisible in PIPICO but readily visible in PEPIPICO, is only a few percent of the ion-pair signal.

PEPIPICO

The PEPIPICO spectrum measured at 305 eV ($C\ 1s \rightarrow \sigma^*$ resonance maximum) under weak extraction field conditions and with the lens operated in defocus mode, using the voltages displayed in the first row of Table 2, is presented in Fig. 9 in comparison to the PIPICO spectrum recorded at the same time. The defocus mode with a weak extraction field is the best condition for examining kinematics of ionic frag-

mentation since these conditions provide the largest sensitivity to kinetic energy and angular distributions. Figure 9 illustrates clearly the advantage of PEPIPICO relative to PIPICO. A total of four distinct ion-pair signals are clearly observed by PEPIPICO, whereas only two distinct signals are detected in the PIPICO signal recorded simultaneously. The (O^{++}, C^+) signal is clearly observed in PEPIPICO, whereas it is masked by the much stronger (C^+, O^+) signal in PIPICO. The very weak (C^{++}, O^{++}) signal from quadruple ionization is also clearly detected. Figure 9 also illustrates the power of the defocus mode to reveal details of the kinetic energy release distributions. The differences in the slope of the major axis of the coincidence signal are trivially related to the changes in the charge state of the ions in-

volved (1), since the events are pair dissociations in which all particles are detected. The separation of the two peaks along the major axis is related to the average kinetic energy release, which is significantly larger for 2+/1+ than for 1+/1+ and larger again for 2+/2+ charge separation. Detailed analysis of the full line shape (1) provides quantitative kinematic information, which can be compared to computed potential energy surfaces of CO⁺⁺ (6).

Summary

Three different operation modes of a newly installed ion lens were found, corresponding to conditions predicted from SIMIONTM simulations. The focus mode was found to produce yields that have minimal kinetic energy or angular discrimination and thus are likely to correspond to the true quantitative yields. The photoion branching ratios for C 1s and O 1s excited and ionized CO were measured in the focus mode and converted to absolute partial ion yield oscillator strengths. When compared with an early literature result (6), claimed to be quantitative, we find significant differences in the individual ion yields. While we believe the present system operated in the focus mode provides more quantitative ion yields than the method used in the earlier study, beamline-specific factors such as interference from stray light or residual second-order radiation may still have distorted the results presented in this work. Comparison to other independent photoionization or (e,e + ion) coincidence measurements with mass spectrometers optimized for quantitative results is required to properly establish the accuracy of these results. We encourage other researchers to provide such results. In the meanwhile, we will continue to use our apparatus in the focus mode to study the photon energy dependence of molecular photofragmentation in our ongoing search for X-ray selective photochemistry.

Acknowledgements

This research is supported financially by the Natural Sciences and Engineering Research Council of Canada (NSERC), the Canada Research Chair program, and Fundação Universitária José Bonifácio (FUJB) (Brazil). Joselito Maciel acknowledges support of a Fundação de Amparo à Pesquisa do Estado do Rio de Janeiro (FAPERJ) postdoctoral fellowship, Antonio Guerra gratefully acknowledges a Comissão de Aperfeiçoamento de Pessoal de Nível Superior (CAPES) graduate fellowship, and Rene Bilodeau acknowledges an NSERC postdoctoral fellowship. The Synchrotron Radiation Center is funded by the National Science Foundation (award No. DMR-0084402) and operated by the Graduate School of the University of Wisconsin-Madison. We thank Yong-Feng Hu, Astrid Jurgensen, and Kim Tan of the SRC-based Canadian Synchrotron Radiation Facility for assistance with operation of the TOF on the SGM.

References

1. A.P. Hitchcock and J.J. Neville. *In* Chemical applications of

synchrotron radiation. *Edited by* T.K. Sham. World Scientific, Singapore. 2001.

2. W. Eberhardt, T.K. Sham, R. Carr, S. Krummacher, M. Strongin, S.L. Weng, and D. Wesner. *Phys. Rev. Lett.* **50**, 1038 (1983); W. Eberhardt and T.K. Sham. *Proc. SPIE*, **447**, 143 (1984).
3. W.C. Wiley and H. McLaren. *Rev. Sci. Instrum.* **26**, 1150 (1955).
4. J.B. Maciel, E. Morikawa, and G.G.B. de Souza. Presented at the 10th US National Conference on Synchrotron Radiation Instrumentation, Ithaca, NY, 1997; A.C.F. Santos, C.A. Lucas, and G.G.B. de Souza. *Chem. Phys.* **282**, 315 (2002).
5. D.A. Dahl. SIMION 3D. Version 6.0 [computer program]. Ion Source Software, PO Box 2726, Idaho Falls, ID 83403.
6. A.P. Hitchcock, P. Lablanquie, P. Morin, M. Simon, E. Lizon, A. Lugin, P. Thiry, and I. Nenner. *Phys. Rev. A*, **37**, 2448 (1988).
7. R.B. Kay, P.E. Van der Leeuw, and M.J. Van der Wiel. *J. Phys. B*, **10**, 2521 (1977).
8. W.C. Stolte, D.L. Hansen, M.N. Piancastelli, I. Dominguez Lopez, A. Rizvi, O. Hemmers, H. Wang, A.S. Schlachter, M.S. Lubell, and D.W. Lindle. *Phys. Rev. Lett.* **86**, 4504 (2001).
9. N. Saito, F. Heiser, O. Hemmers, A. Hempelmann, K. Wieliczek, J. Viehhaus, and U. Becker. *Phys. Rev. A*, **51**, R4313 (1995).
10. M. Benndorf, W.B. Westerveld, J. van Eck, J. van der Weg, and H.G.M. Heideman. *J. Phys. B*, **32**, 2503 (1999).
11. P. Erman, A. Karawajczyk, E. Rachlew-Källne, and C. Strömholm. *J. Phys. B*, **28**, 2069 (1995).
12. P. Erman, A. Karawajczyk, U. Köble, E. Rachlew-Källne, and K. Yoshiki Franzén. *Phys. Rev. A*, **53**, 1407 (1996).
13. N. Saito, F. Heiser, O. Hemmers, K. Wieliczek, J. Viehhaus, and U. Becker. *Phys. Rev. A*, **54**, 2004 (1996).
14. N. Saito, A. Hempelmann, F. Heiser, O. Hemmers, K. Wieliczek, J. Viehhaus, and U. Becker. *Phys. Rev. A*, **61**, 022709 (2000).
15. F. Heiser, O. Geßner, J. Viehhaus, K. Wieliczek, R. Hentgens, and U. Becker. *Phys. Rev. Lett.* **79**, 2435 (1997).
16. O. Gessner, F. Heiser, N.A. Cherpkov, B. Zimmermann, and U. Becker. *J. Electron. Spectrosc.* **101–103**, 113 (1999).
17. P.A. Hatherly, J. Adachi, E. Shigemasa, and A. Yagishita. *J. Phys. B*, **28**, 2643 (1995).
18. A. Hamnett, W. Stoll, and C.E. Brion. *J. Electron. Spectrosc.* **8**, 367 (1976).
19. W.B. Westerveld, J. van der Weg, J. van Eck, H.G.M. Heideman, and J.B. West. *Chem. Phys. Lett.* **252**, 107 (1996).
20. M.J. Van Der Wiel, Th.M. El-Sherbini, and C.E. Brion. *Chem. Phys. Lett.* **7**, 161 (1970).
21. G.R. Wight, C.E. Brion, and M.J. Van Der Wiel. *J. Electron. Spectrosc.* **1**, 457 (1972/1973).
22. R.B. Kay, P.E. Van der Leeuw, and M.J. Van der Wiel. *J. Phys. B*, **10**, 2513 (1977).
23. M. Tronc, G.C. King, and F.H. Read. *J. Phys. B*, **12**, 137 (1979).
24. A.P. Hitchcock and C.E. Brion. *J. Electron. Spectrosc.* **18**, 1 (1980).
25. I. Nenner. *In* Proc. XV Int. Conf. Photon, Electron and Atomic Collisions (ICPEAC), Brighton, UK, 1987. Plenum Press, New York. 1988. p. 15.
26. T.A. Carlson and R.M. White. *J. Chem. Phys.* **44**, 4510 (1966).
27. A.P. Hitchcock. Data base of absolute photoabsorption cross sections for gaseous species [online]. Available from <http://unicorn.mcmaster.ca/corex.html>. (2003).